Electronic Supplementary Material (ESI) for Nanoscale.

Electronic Supplementary Information

Processable Dispersions of Photocatalytically Active Nanosheets derived from Titanium diboride: Self Assembly into Hydrogels and Paper-like Macrostructures

*Asha Liza James †, Manis Lenka †, Nidhi Pandey †, Abhijeet Ojha ‡, Ashish Kumar §, Rohit Saraswat †, Prachi Thareja †, Venkata Krishnan §, and Kabeer Jasuja †**

†Discipline of Chemical Engineering, Indian Institute of Technology Gandhinagar, Palaj, Gujarat 382355, India

‡Discipline of Biological Engineering, Indian Institute of Technology Gandhinagar, Palaj, Gujarat 382355, India

§School of Basic Sciences and Advanced Materials Research Center, Indian Institute of Technology Mandi, Kamand, Mandi, Himachal Pradesh 175075, India

Sections:

1. Physico-chemical Characterization
    1.1 Microscopic Characterization of Standard TiB_2
    1.2 Characterization of Nanosheets derived from TiB_2
2. Hydrogels formed from aqueous dispersions of nanosheets derived from TiB_2
3. Assembling Paper-like Macrostructures
    3.1 Free-standing paper like films from nanosheets derived from TiB_2
    3.2 Hybrid paper-like structures composed of graphene oxide and TiB_2 derived nanosheets
4. Photocatalytic action of the TiB_2 derived nanosheets

Section 1: Physico-chemical Characterization

1.1 Microscopic Characterization of Standard TiB_2

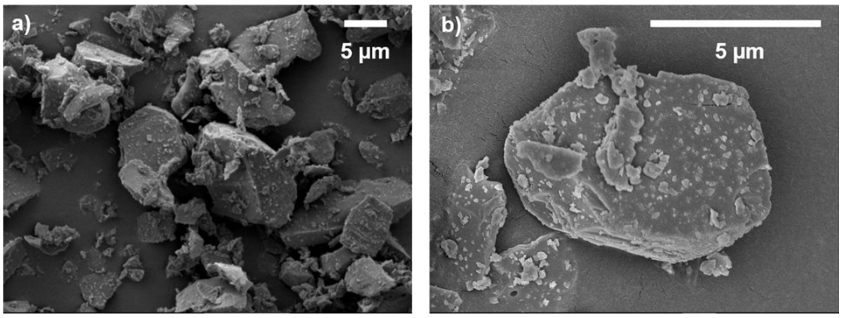

Figure S1: FESEM images of the standard TiB_2 particles, as obtained from the chemical vendor (designated as particles size <10 µm). The particles were dusted on conducting carbon tape prior to analysis under the FESEM.

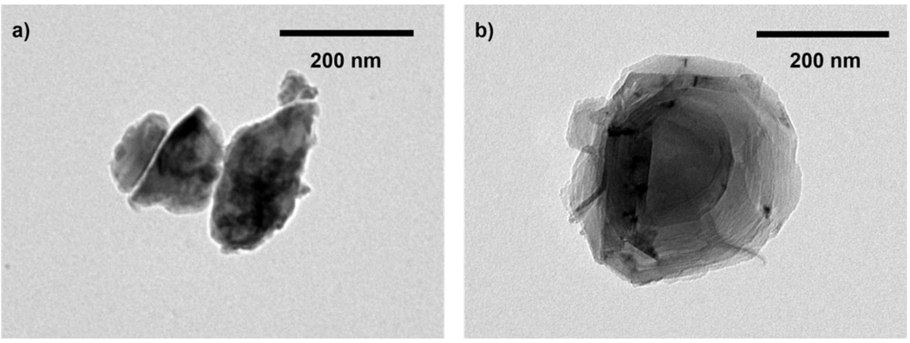

Figure S2: TEM images of the as obtained TiB_2 particles, dispersed in ethanol and dropcasted on carbon coated Cu grids.

1.2 Characterization of Nanosheets derived from TiB_2

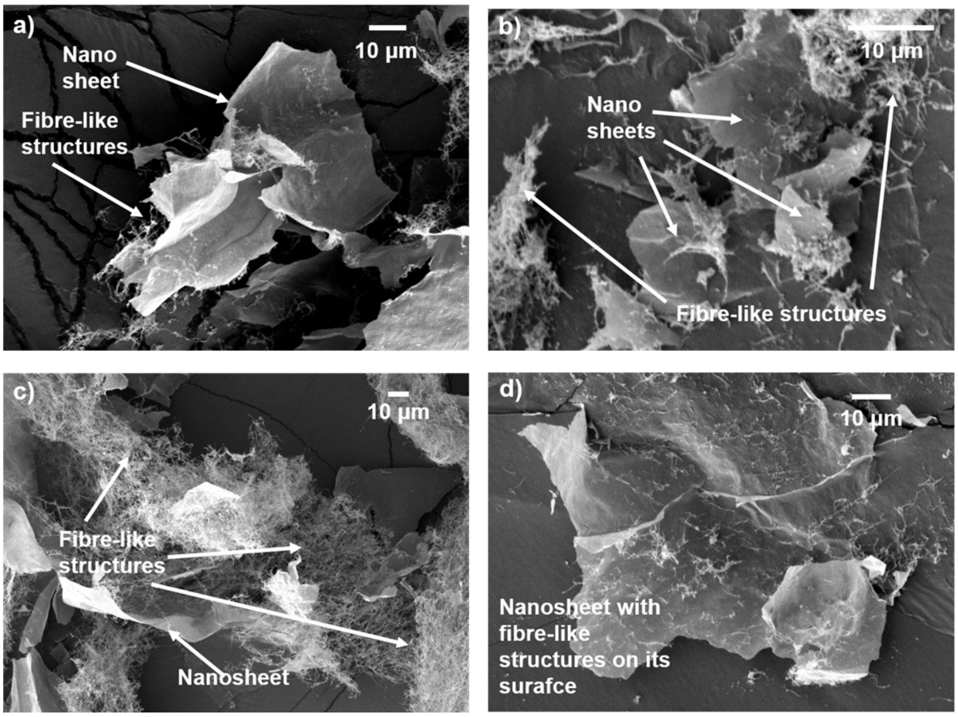

Figure S3: FESEM of the lyophilized powder-form of the nanosheets, showing the presence of fiber-like structures.

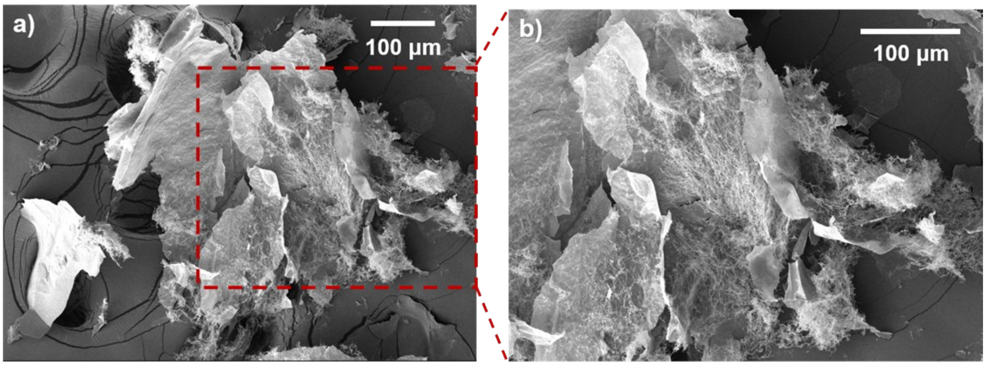

Figure S4: FESEM of the lyophilized powder-form of the nanosheets, showing the presence of fiber-like structures.

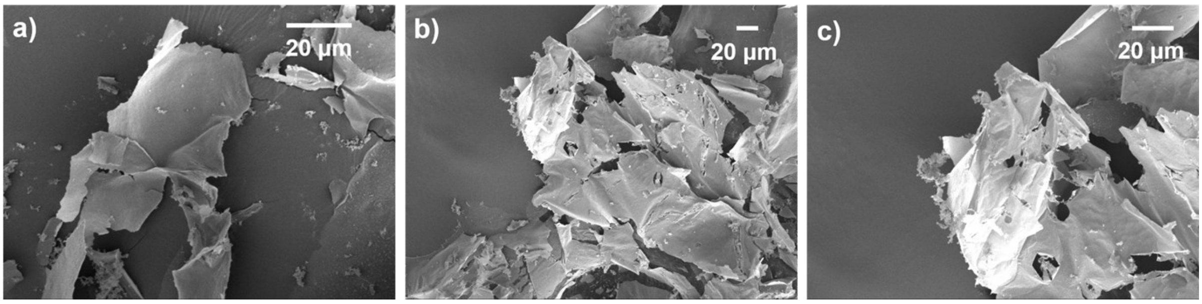

Figure S5: FESEM of the lyophilized powder-form of the nanosheets obtained after dialysis.

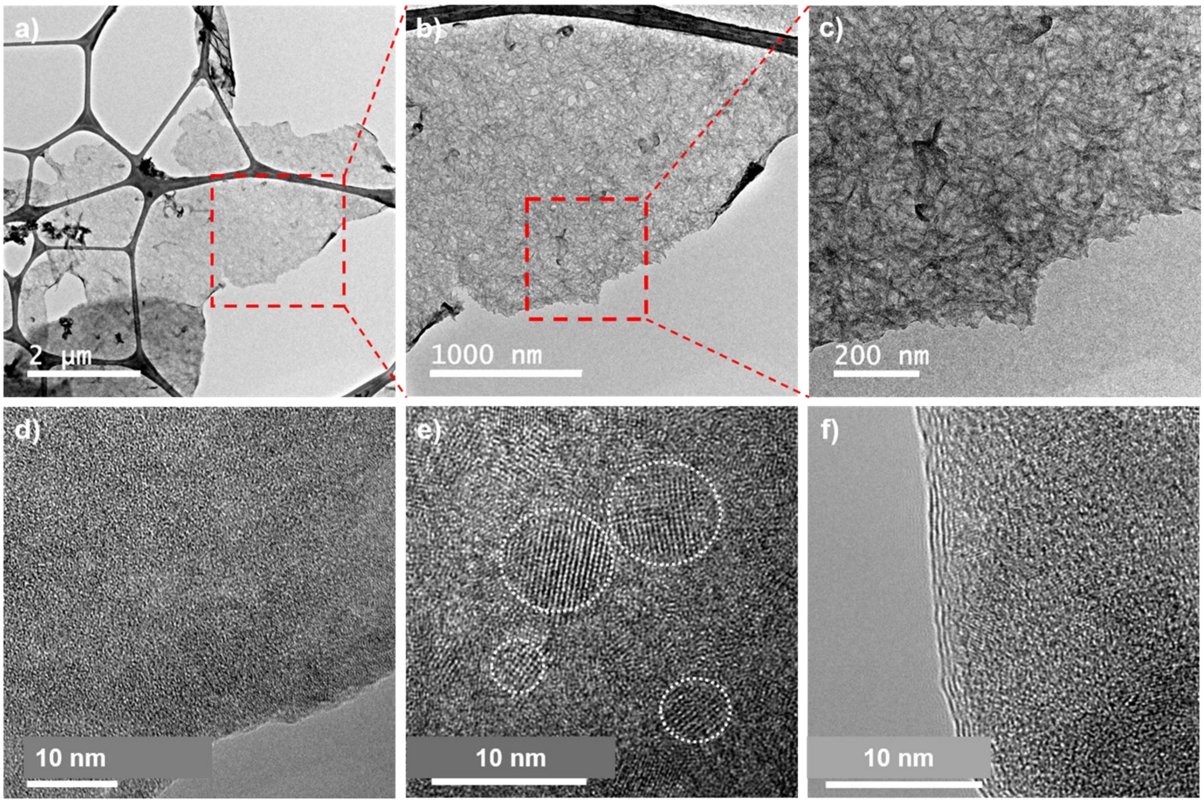

Figure S6: HRTEM studies of the powder form of the nanosheets re-dispersed in water and deposited onto the Cu grids.

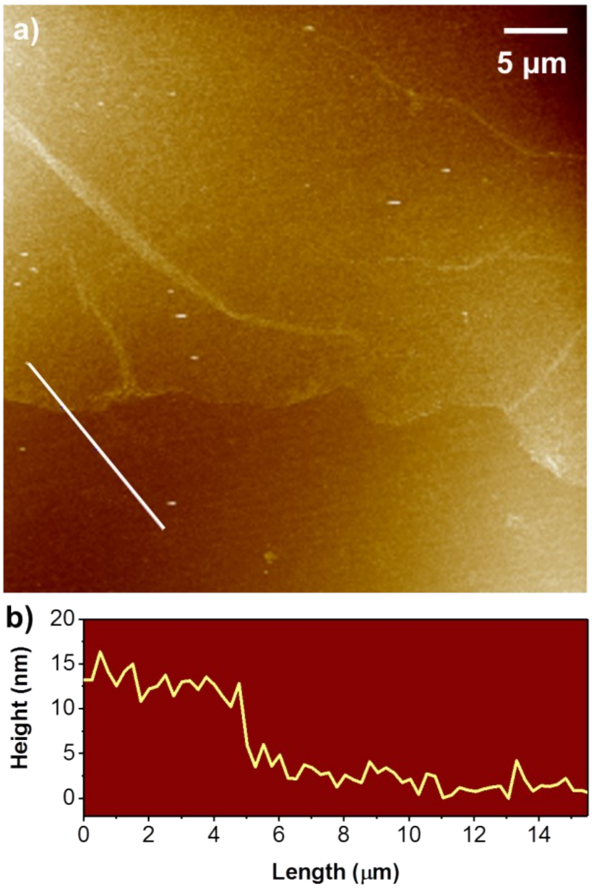

Figure S7: AFM image showing the edge of an ultra-large sheet and the height profile corresponding to the line marked on the sheet, indicating a thickness < 10 nm.

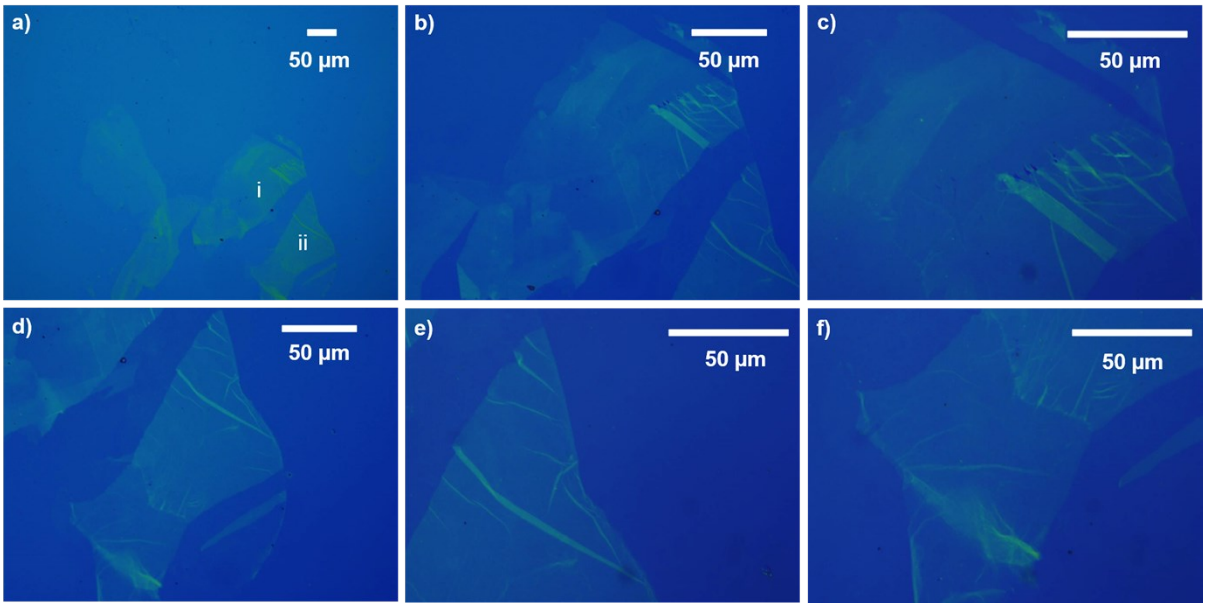

Figure S8: Optical micrographs of the nanosheets deposited on Si/SiO$_2$ wafer. Nanosheet marked as (i) is subsequently zoomed in images b and c; nanosheet marked as (ii) is zoomed and shown in d, the top part and bottom part of this sheet are further zoomed in e and f respectively.

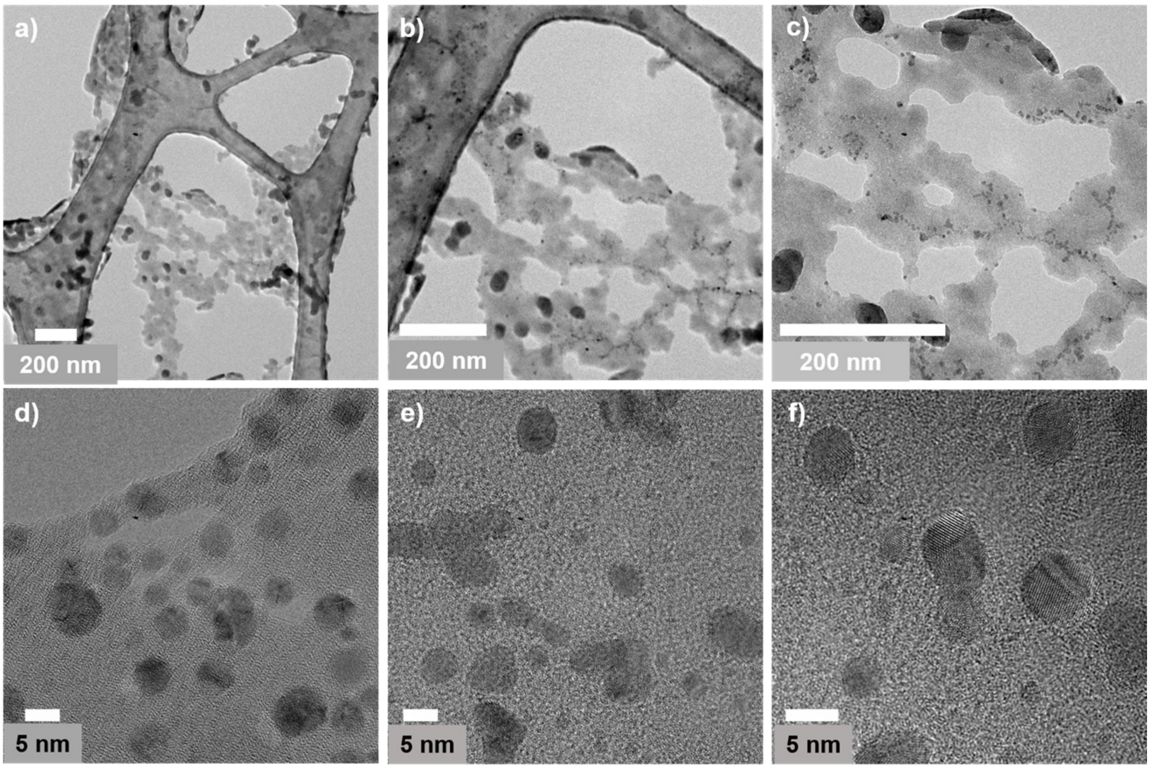

Figure S9: TEM (a-c) and HRTEM (d-f) images of the samples drawn at the beginning of reaction.

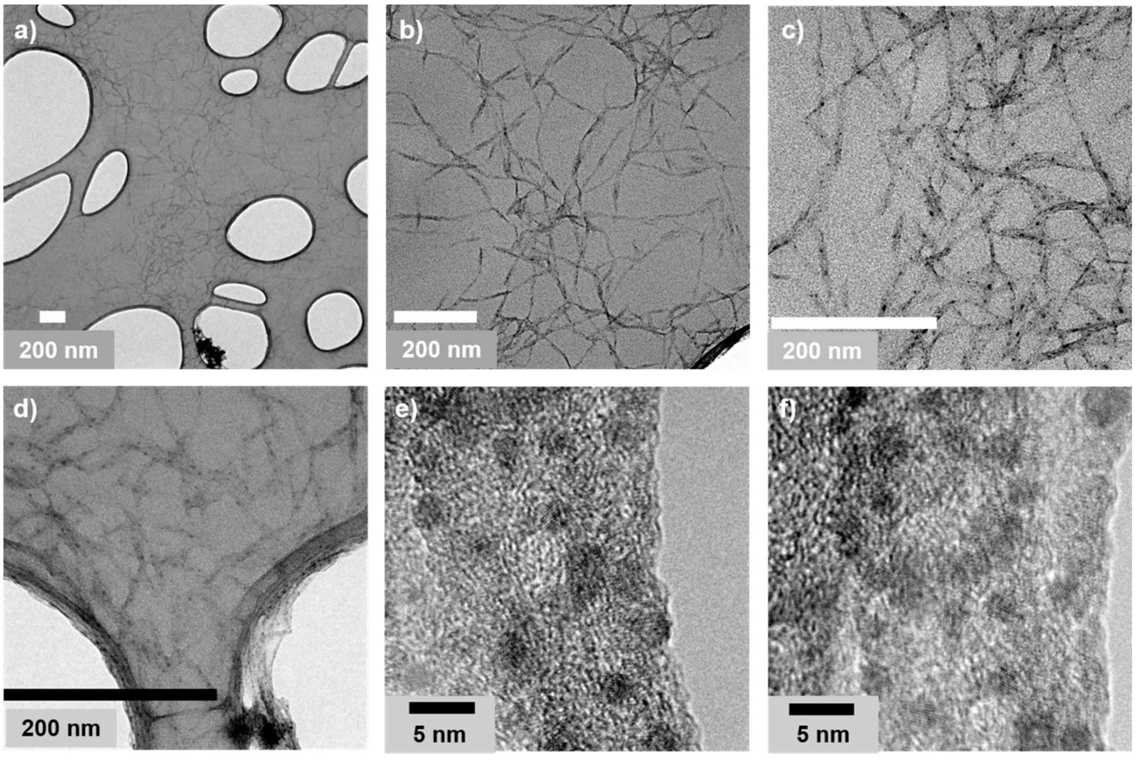

Figure S10: TEM (a-d) and HRTEM (e-f) images of sample drawn after completion of reaction.

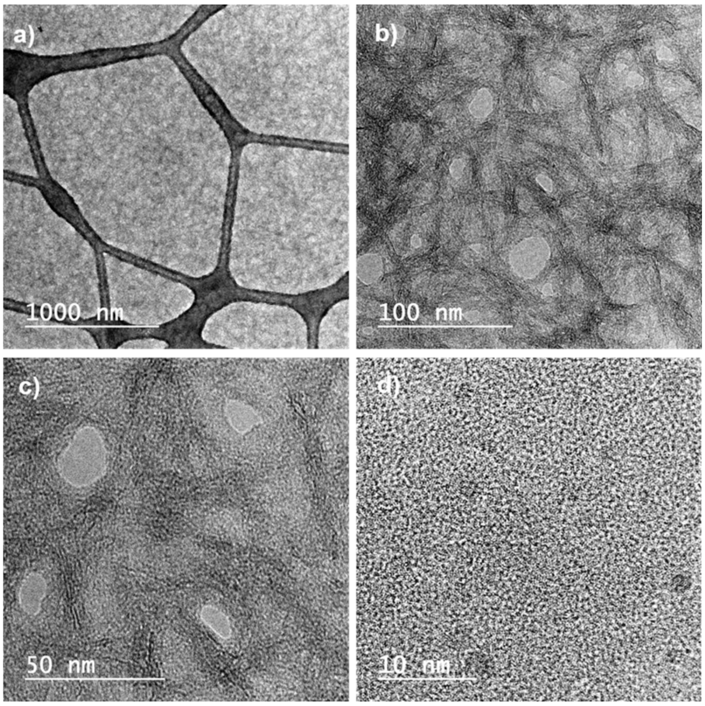

Figure S11: TEM and HRTEM studies of the sample drawn after 4 hours of reaction. Upon zooming in on the low magnification image in a), fibrous structures are seen as shown in b). The high resolution image of a region in b) is depicted in c). The further zoomed in image in d) shows presence of particulate species which are prenucleation clusters.

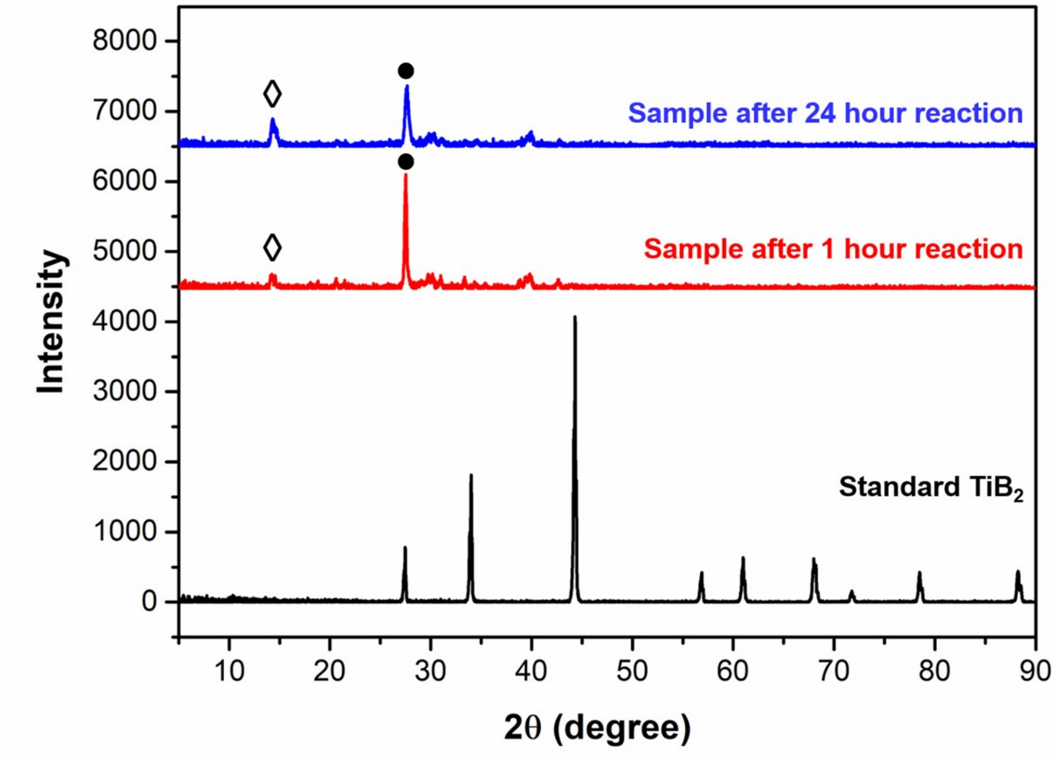

Figure S12: XRD patterns of standard TiB_2 powder and the sample after 1 hour and 24 hours of reaction affirm the oxidative attack of H_2O_2. The ◊ symbol indicates H_3BO_3 and ● indicates titanium dioxide (rutile) compounds (JCPDS card no. 73-2158 and JCPDS card no. 21-1276 respectively).

X-ray diffraction studies of the TiB_2 nanosheets helped us obtain more insights into the interaction of TiB_2 with aqueous H_2O_2. Liu *et al.* in their study of acidic hydrolysis of TiB_2 in water, have reported that the TiB_2 undergoes a layer-by-layer dissolution.[1] The surface Ti is prone to readily adsorb OH from water and owing to surface hydrolysis, water soluble Ti complexes form spontaneously. Such a dissolution of TiB_2 is followed by the nucleation and subsequent growth of TiO_2 species.[1] They also comment on the fate of the 2D boron networks in the TiB_2 undergoing dissolution as follows. Ti complex formation alters the coordination state of boron, which favors the adsorption of OH group onto the boron atoms. In acidic media, the hydroxylated boron species eventually forms stable H_3BO_3, the evidence for which was observed from XRD analysis of the byproduct after the hydrothermal hydrolysis of TiB_2, as explained ahead. The XRD patterns of the lyophilized powder form of the reaction mixture recovered after 1 hour and 24 hours of reaction are compared with that of standard TiB_2 in Fig. S9 in the ESI. The peak corresponding to the (001) plane in TiB_2 ($2\theta = 27.5^0$) is gradually falling in intensity, with a concomitant increase in a new peak around $2\theta = 12.4^0$ which corresponds to H_3BO_3. It may be noted that the diffraction pattern of the samples could not be completely matched with any compound in the database. The peak corresponding to ~27^0 in the samples withdrawn after reaction, could also be indexed to (110) plane of rutile TiO_2, in line with the hydrolysis of TiB_2 as outlined earlier in this paragraph. The major peaks may be hence assigned to TiB_2, TiO_2 and H_3BO_3. The contributions from the latter become more prominent after the reaction with H_2O_2 happens. It may also be noted that literature pertaining to the interaction of TiB_2 with H_2O_2 or the hydrolysis of TiB_2, often comment that the oxides of boron are present separately in the aqueous phase. But it may be noted that, even after 24 hours of dialysis the oxy-boron species have not been removed from the sample indicating they are a structural part of the nanosheets.

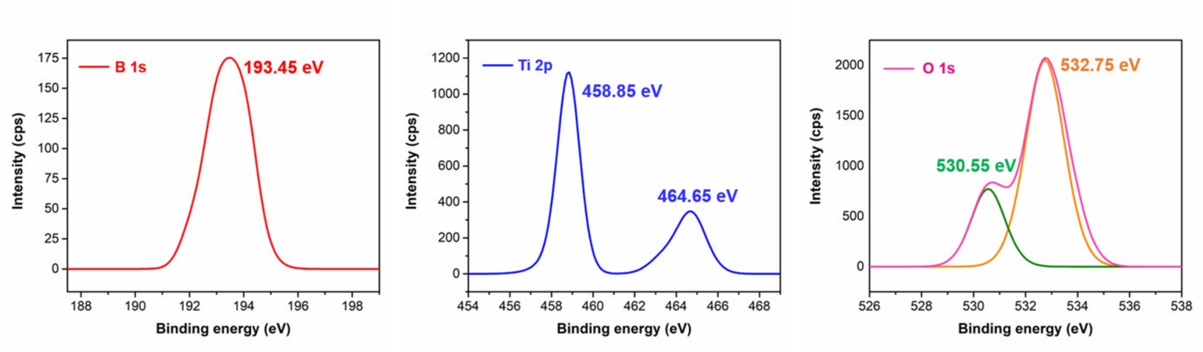

Figure S13: XPS spectra of samples after 4 hours of reaction

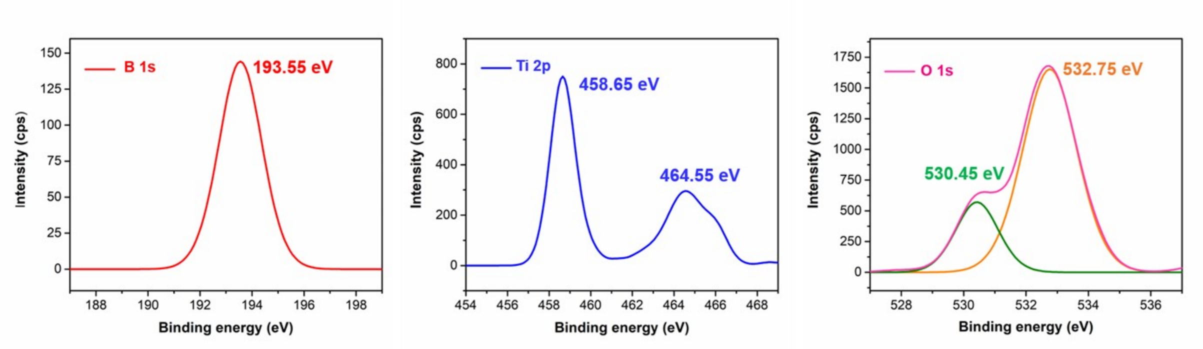

Figure S14: XPS spectra of samples after 24 hours of reaction

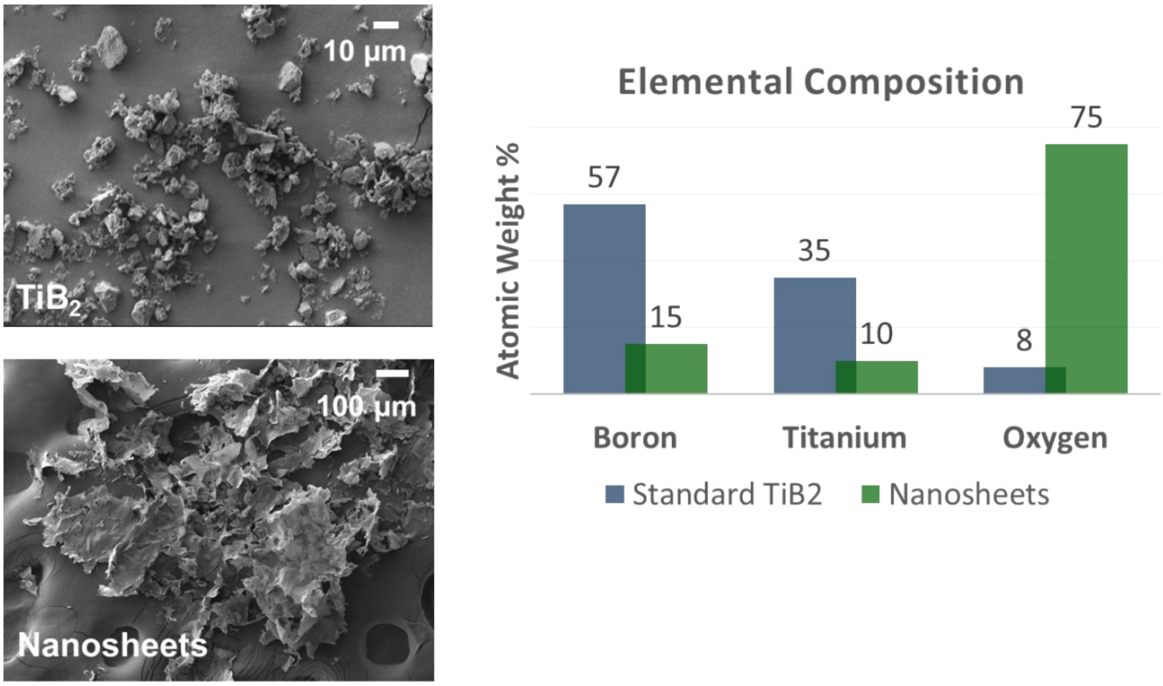

Figure S15: FESEM/EDX of standard TiB_2 and the lyophilized powder-form of the nanosheets.

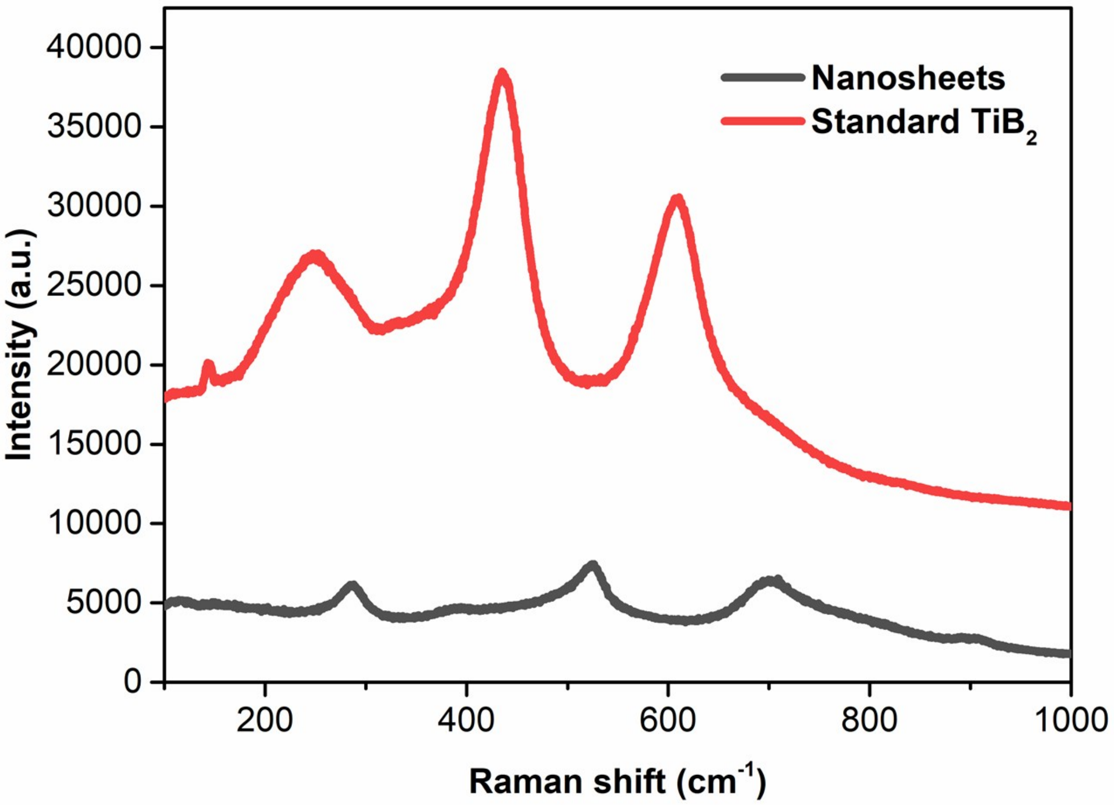

Figure S16: Comparison of Raman spectra of standard TiB_2 and nanosheets derived from TiB_2.

Section 2: Hydrogels formed from aqueous dispersions of nanosheets derived from TiB_2

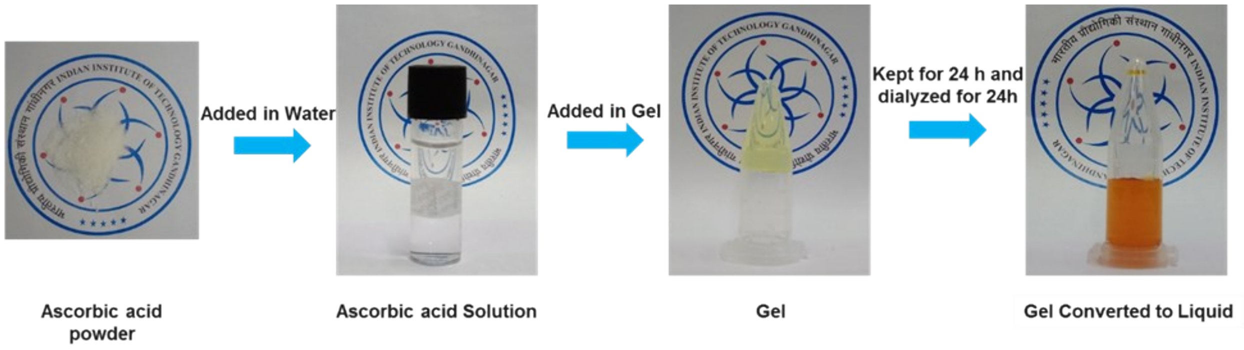

Figure S17: Addition of a reducing agent, ascorbic acid, results in a chemical action on the gel sample, transforming it into a liquid-like state, with an associated color change from yellow to bright orange.

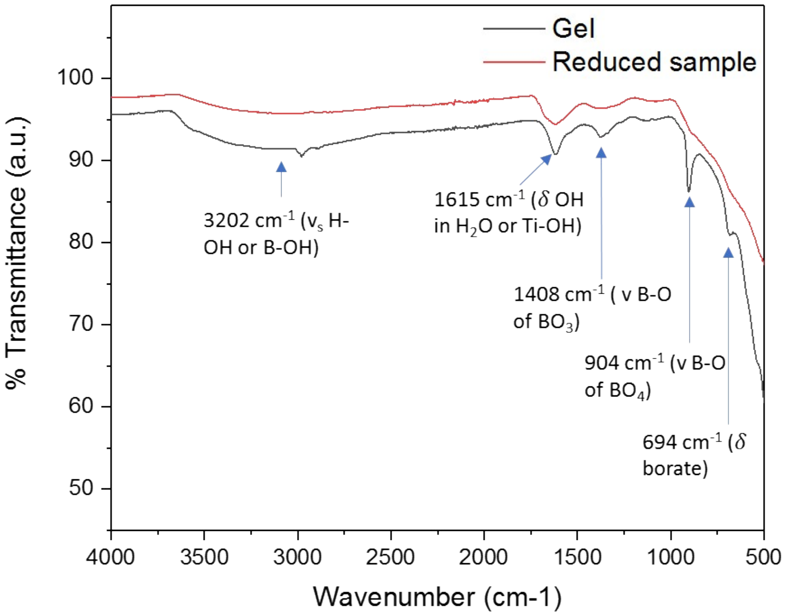

Figure S18: FTIR spectra of the gel and reduced sample are compared; the intensity of the boron-oxy functional groups have decreased indicating that the loss of gel-like properties could be due to the disappearance of the borate based cross linking upon chemical reduction.

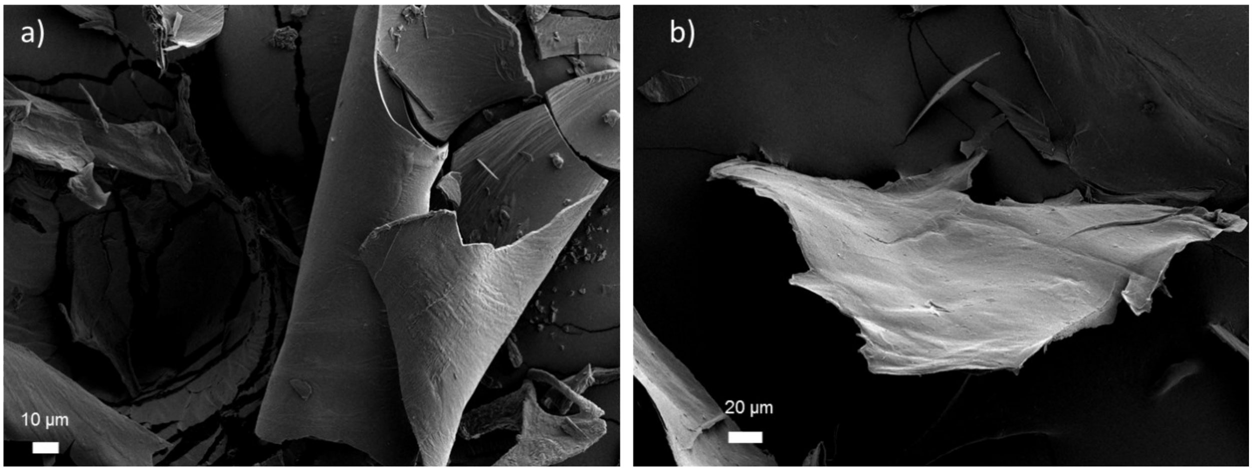

Figure S19: FESEM of the reduced samples; (a) morphology of the reduced sample, (b) morphology of the reduced sample after dialysis.

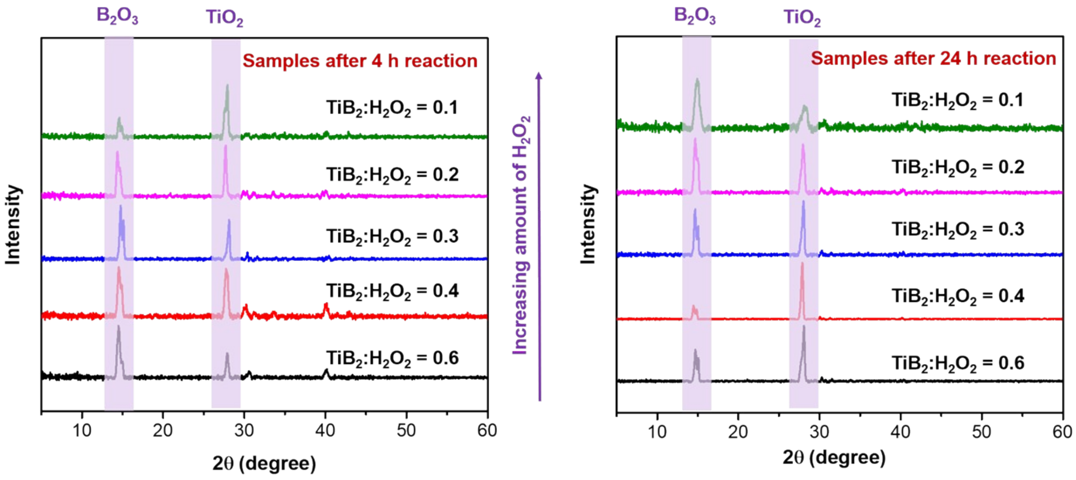

Figure S20: XRD patterns of samples withdrawn after 4 hour and 24 hour reaction corresponding to different $TiB_2:H_2O_2$ ratios. (Kindly note that the patterns are normalized and hence do not feature the Y-axis values.)

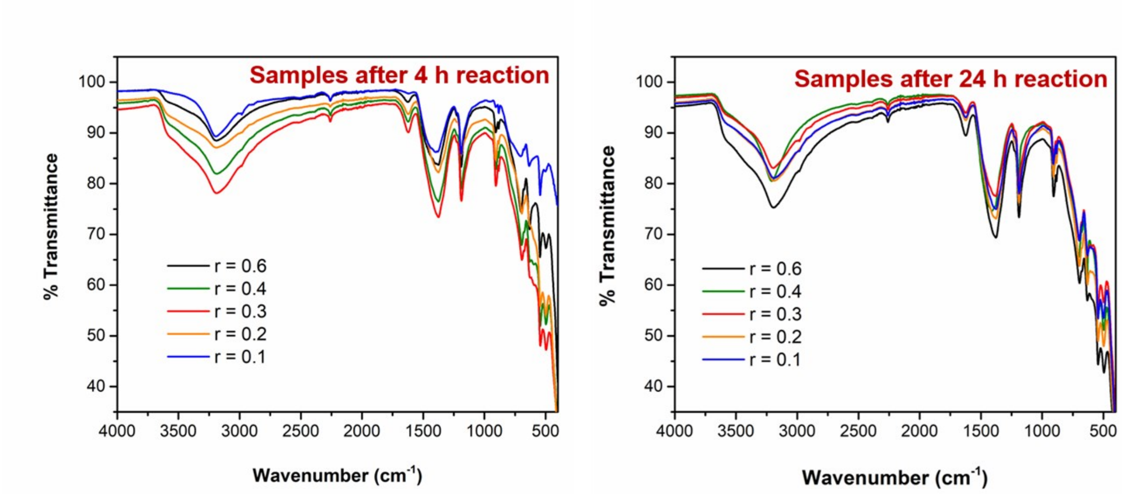

Figure S21: FTIR spectra of samples after 4 hour and 24 hour reaction corresponding to different $TiB_2:H_2O_2$ ratios

Section 3: Assembling Paper-like Macrostructures

3.1 Free-standing paper like films from nanosheets derived from TiB_2

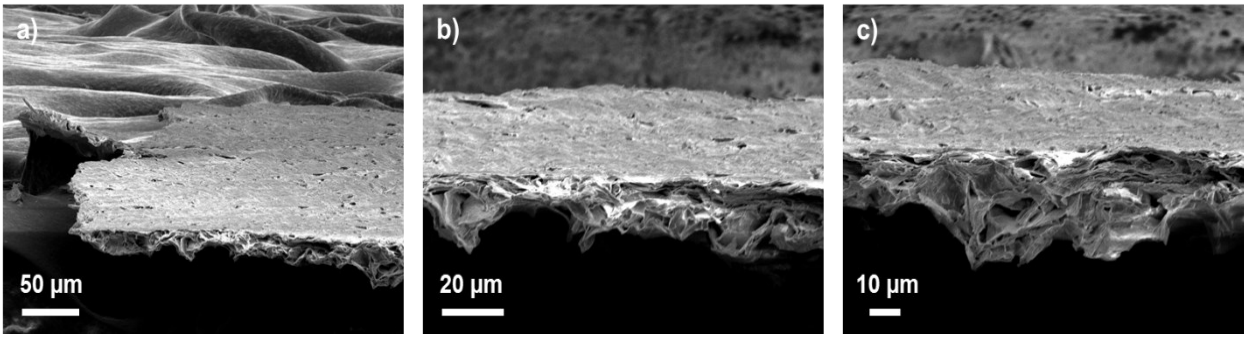

Figure S22: FESEM imaging of a fractured piece of the free-standing paper show the hierarchical assembly of the nanosheets in a layer-by-layer arrangement. The figures b and c are zoomed in versions of the structure depicted in Figure S22a.

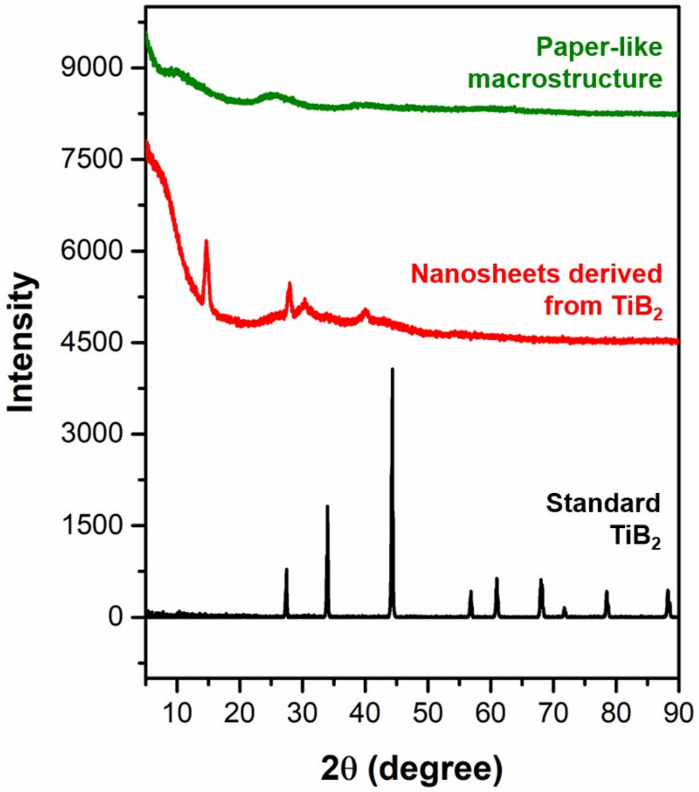

Figure S23: XRD analysis of TiB_2 powder, TiB_2 based nanosheets and free-standing paper-like film of TiB_2 based nanosheets.

Section 3.2 Hybrid paper-like structures composed of graphene oxide and TiB_2 derived nanosheets

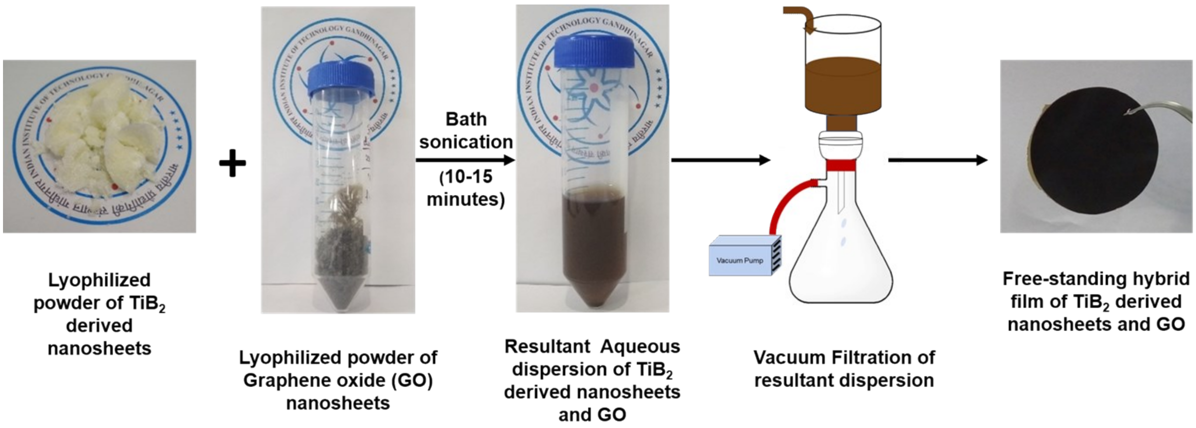

Figure S24: Mixed dispersions of nanosheets derived from TiB_2 and GO nanosheets upon vacuum filtration also form free standing hybrid films.

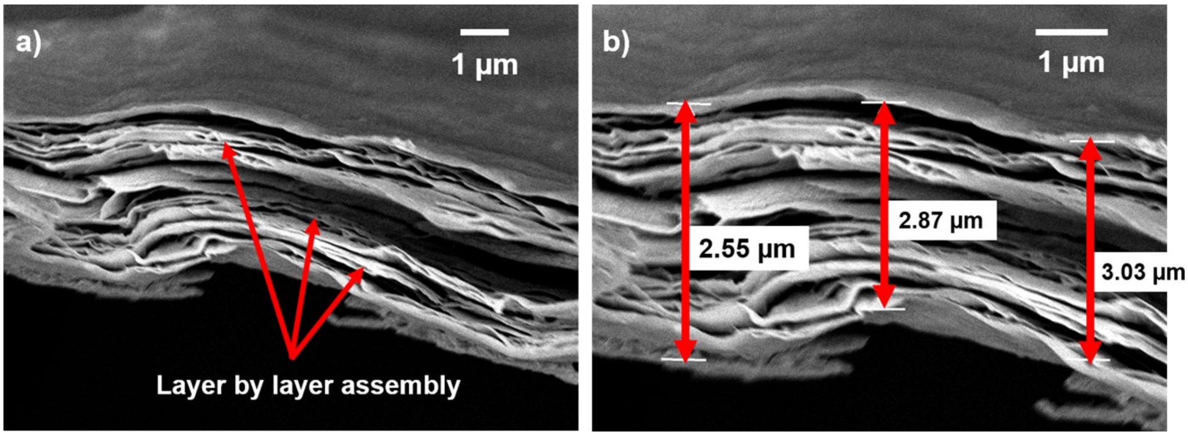

Figure S25: FESEM imaging of the hybrid films reveal the layer-by-layer assembly

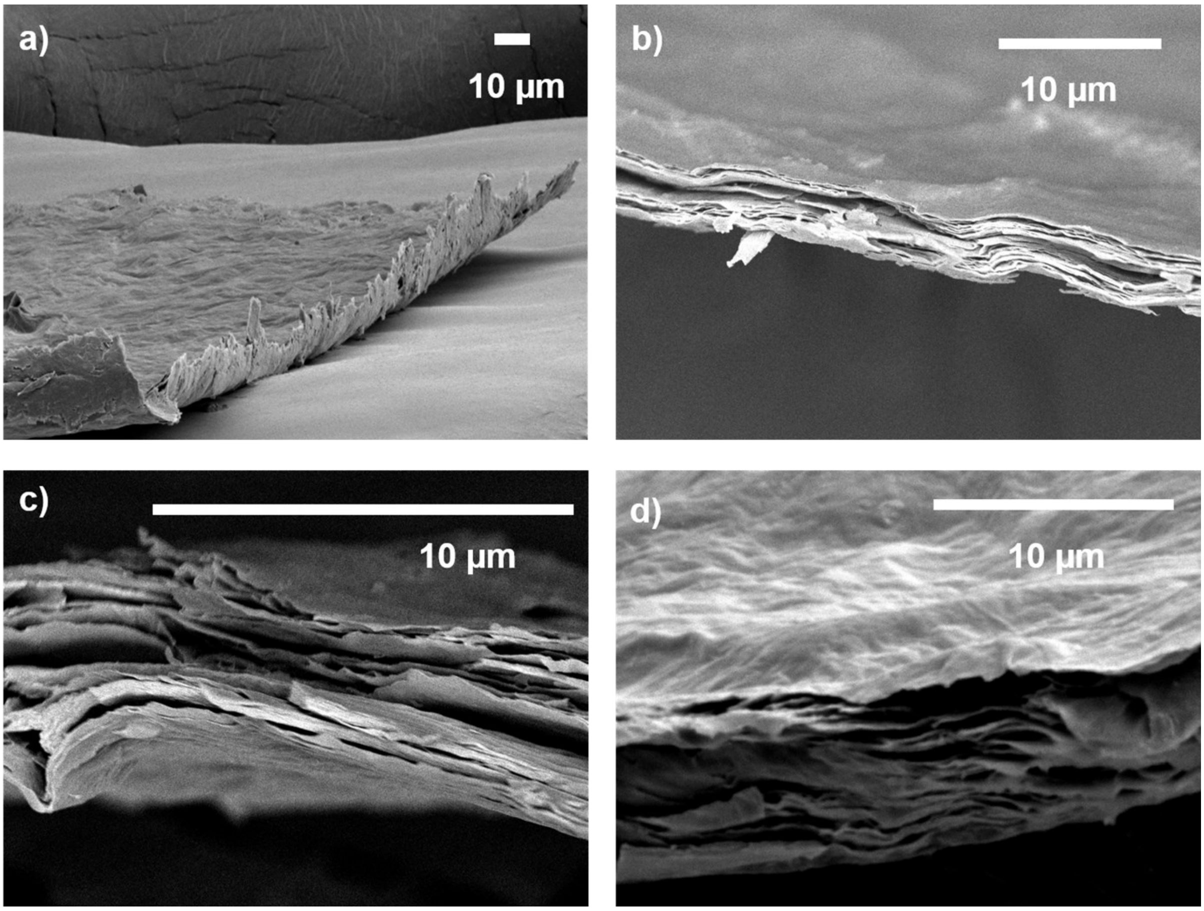

Figure S26: FESEM imaging of the GO nanosheet-TiB_2 derived nanosheet hybrid films: (a) a piece of the film on conducting carbon film; (b) view of the edge of the film; (c-d) closer view of the edge showing layer by layer arrangement of sheet like structures

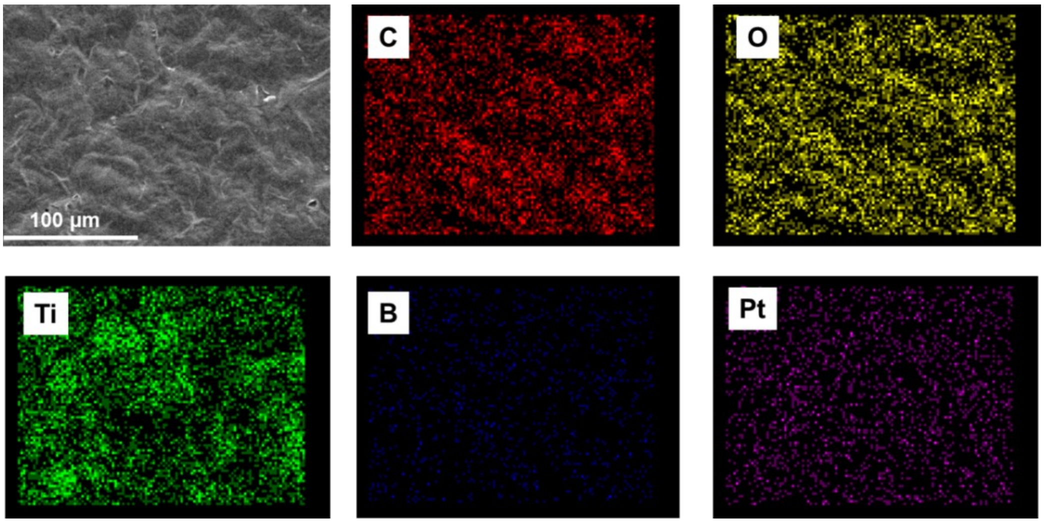

Figure S27: FESEM-EDX elemental mapping of the hybrid film of graphene oxide/TiB_2 derived nanosheets which shows the distribution of elements carbon (C), oxygen (O), titanium (Ti), Boron (B) and Platinum (Pt - due to platinum sputtering) in the hybrid film.

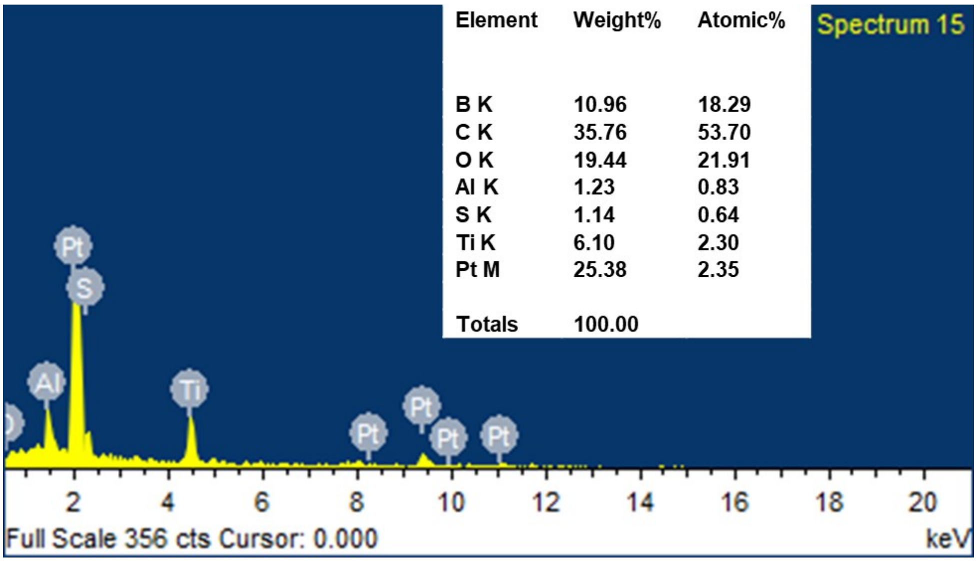

Element	Weight%	Atomic%
B K	10.96	18.29
C K	35.76	53.70
O K	19.44	21.91
Al K	1.23	0.83
S K	1.14	0.64
Ti K	6.10	2.30
Pt M	25.38	2.35
Totals	100.00	

Figure S28: EDX spectrum of the hybrid film of graphene oxide nanosheets with TiB_2 based nanosheets depicts the presence of carbon, boron, oxygen, aluminum (due to Anodisc membrane used for filtration), titanium, sulfur (from modified Hummer's method used in GO synthesis), and platinum (Pt sputtering).

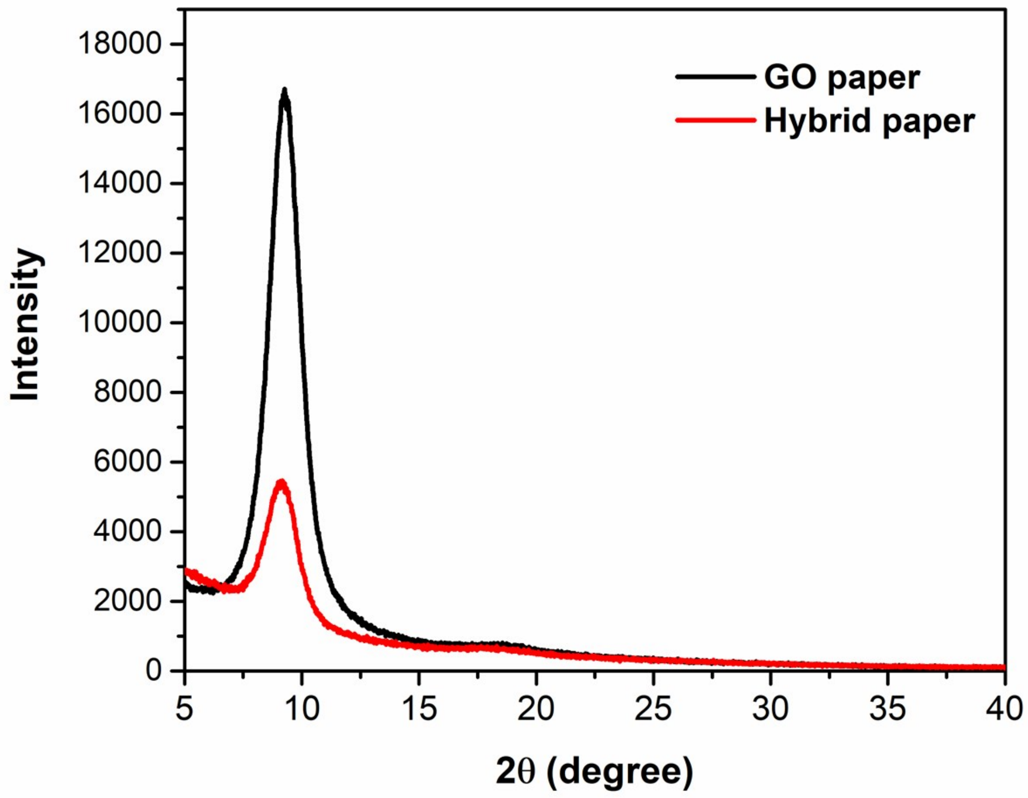

Figure S29: XRD patterns of GO paper and hybrid paper.

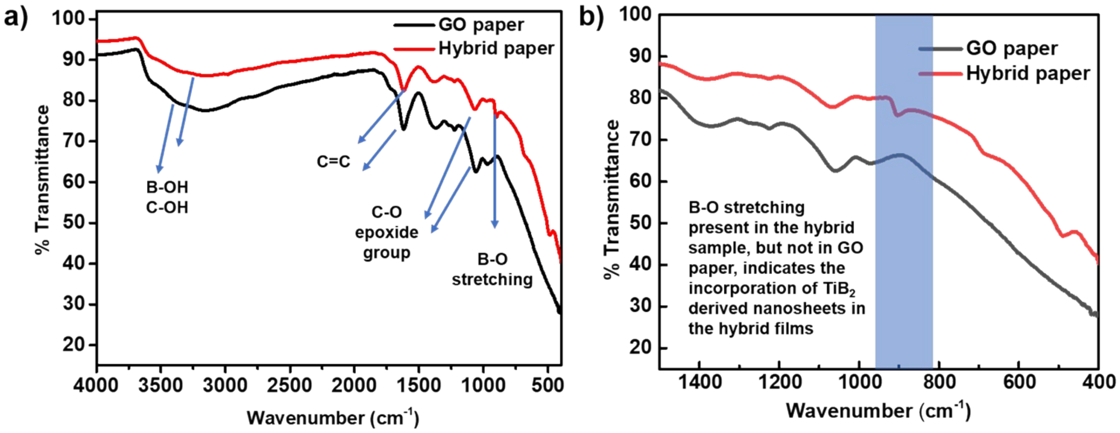

B-O stretching present in the hybrid sample, but not in GO paper, indicates the incorporation of TiB_2 derived nanosheets in the hybrid films

Figure S30: FTIR spectra comparison of the film of GO nanosheets and hybrid film prepared from the mixture of TiB_2 based nanosheets and GO nanosheets. FTIR spectra of both the films show almost the same peaks because most of the chemical functionalization of boron and carbon lies in the same region. However, B-O stretching peak is present only in the hybrid paper as shown in b), indicating presence of TiB_2 derived nanosheets in the hybrid.

Section 4: Photocatalytic action of the TiB_2 derived nanosheets

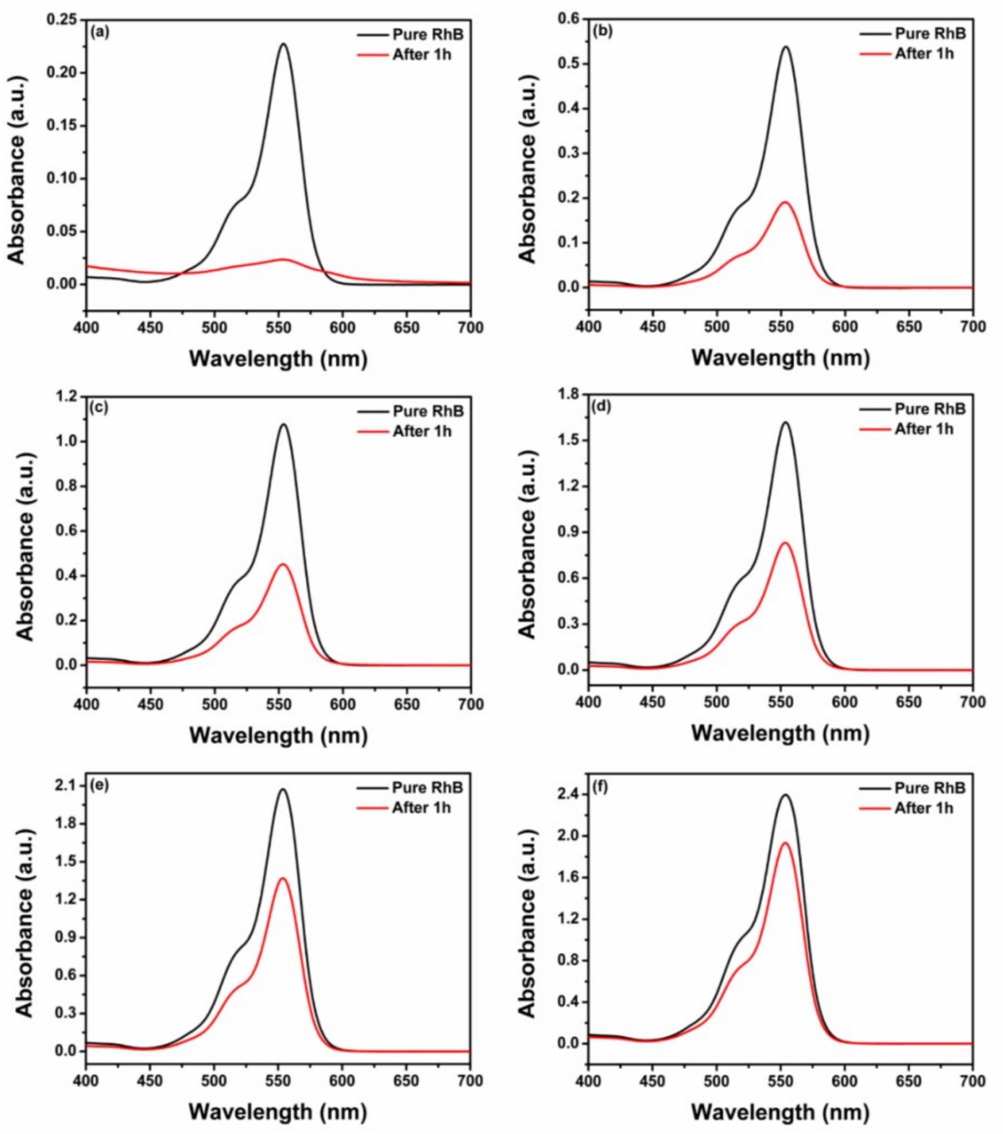

Figure S31: Dark adsorption on TiB_2 derived nanosheets of different RhB concentrations (a) 5 µM, (b) 10 µM, (c) 20 µM, (d) 30 µM, (e) 40 µM and (f) 50 µM.

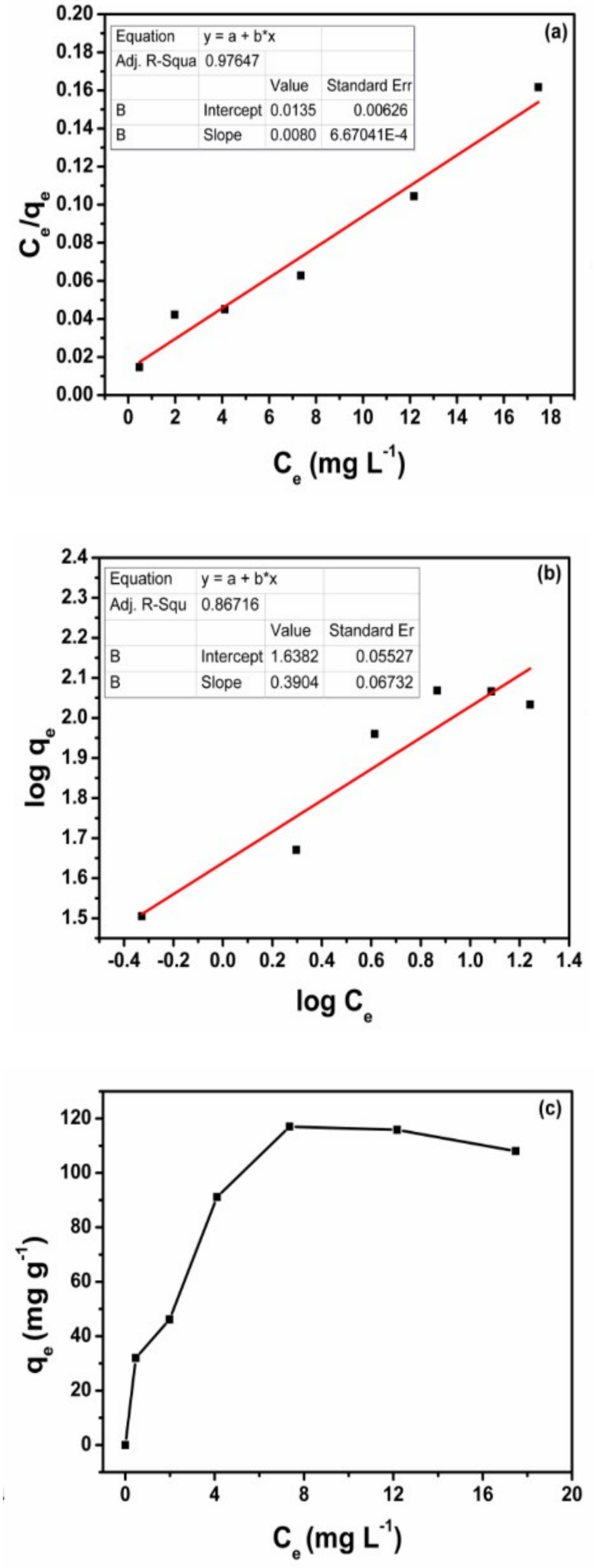

Equation	y = a + b*x		
Adj. R-Squa	0.97647		
		Value	Standard Err
B	Intercept	0.0135	0.00626
B	Slope	0.0080	6.67041E-4

Equation	y = a + b*x		
Adj. R-Squ	0.86716		
		Value	Standard Er
B	Intercept	1.6382	0.05527
B	Slope	0.3904	0.06732

Figure S32: (a) Langmuir adsorption isotherm, (b) Freundlich adsorption isotherm and (c) adsorption capacity for RhB adsorption.

Table S1. Adsorption parameters for RhB on TiB_2 nanosheets.

Langmuir model		
q_m	**K_L**	**R^2**
125.0	0.0001	0.976
Freundlich model		
K_f	**1/n**	**R^2**
43.47	0.3904	0.867

Table S2. Comparison of the adsorption capacity and photocatalytic activity of the TiB_2 derived nanosheets with some adsorptive photocatalysts reported in the recent literature.

Sl. No.	Adsorptive Photocatalyst	Adsorption capacity	Light source	Pollutant (Concentration)	Degradation (Reaction time)	Ref.
1.	$InVO_4/ZnFe_2O_4$	97.1 mg g^{-1}	Vis	MB (25 mg L^{-1})	84.7% (240 min)	2
2.	$NaYF_4$:Yb/Er@ CdS-Au-RGO	9.8 mg g^{-1}	Vis	CFX (5 X 10^{-5} M)	90.0% (180 min)	3
3.	g-C_3N_4-ZnO@graphene	65.8%	Vis	RhB (20 mg L^{-1})	81.0% (120 min)	4
4.	$TiO_2/SiO_2/Ag$	9.2 mg g^{-1}	Vis	OTC (50 ppm)	62.0% (120 min)	5
5.	BiOBr/RGO	24.0%	Vis	RhB (20 mg L^{-1}) TOC=301.2 mg L^{-1}	TOC = 3.7 mg L^{-1} (300 min)	6
6.	N-$CaTiO_3$-RGO	16.0 mg g^{-1}	Vis	MB (4 X 10^{-5} M)	95.0% (180 min)	7
7.	Porous g-C_3N_4	41.0%	Vis	SDZ (10 mg L^{-1})	83.2% (90 min)	8
8.	ZnO/rGO–rGH	65.0%	UV	BPA (10 mg L^{-1})	100% (20 min)	9
9.	TiO_2-Graphene	120.0 mg g^{-1}	UV	MB (10 ppm)	100% (30 min)	10
10.	TiB_2 derived nanosheets	125.0 mg g^{-1}	Natural sunlight	RhB (2 X 10^{-5} M)	92.0% (90 min)	This work
	Ciprofloxacin (CFX), Methylene blue (MB), Oxytetracycline (OTC), Sulfadiazine (SDZ), Bisphenol A (BPA)					

References:

1. G. Liu, H. G. Yang, C. Sun, L. Cheng, L. Wang, G. Q. Lu and H.-M. Cheng, *CrystEngComm*, 2009, **11**, 2677-2682.
2. Z. Wang, J. Wang, Y. Pan, F. Liu, Y. Lai, J. Li and L. Jiang, *Applied Surface Science*, 2020, **501**, 144006.
3. A. Kumar, K. L. Reddy, S. Kumar, A. Kumar, V. Sharma and V. Krishnan, *ACS applied materials & interfaces*, 2018, **10**, 15565-15581.
4. J.-Y. Zhang, J.-Y. Mei, S.-S. Yi and X.-X. Guan, *Applied Surface Science*, 2019, **492**, 808-817.
5. X. Zhao, W. Ju, J. Zhang, B. Liu, J. Zhang and X. Yi, *New Journal of Chemistry*, 2019, **43**, 6234-6241.
6. W. Liu, J. Cai and Z. Li, *ACS Sustainable Chemistry & Engineering*, 2015, **3**, 277-282.
7. A. Kumar, S. Kumar, A. Bahuguna, A. Kumar, V. Sharma and V. Krishnan, *Materials Chemistry Frontiers*, 2017, **1**, 2391-2404.
8. M. Liu, D. Zhang, J. Han, C. Liu, Y. Ding, Z. Wang and A. Wang, *Chemical Engineering Journal*, 2020, **382**, 123017.
9. C. Liu, M. Yue, L. Liu, Y. Rui and W. Cui, *RSC advances*, 2018, **8**, 22402-22410.
10. Z. Zhang, F. Xiao, Y. Guo, S. Wang and Y. Liu, *ACS applied materials & interfaces*, 2013, **5**, 2227-2233.